Electronic Supplementary Information (ESI)

Porous Niobium Nitride as a Capacitive Anode Material for Advanced Li-Ion Hybrid Capacitor with Superior Cycling Stability†

Peiyu Wang‡[ab], Rutao Wang‡[a], Junwei Lang[a], Xu Zhang[a], Zhenkun Chen[a] and Xingbin Yan*[, a]

[a] Laboratory of Clean Energy Chemistry and Materials, State Key Laboratory of Solid Lubrication, Lanzhou Institute of Chemical Physics, Chinese of Academy of Sciences, Lanzhou, 730000, P.R. China

E-mail: xbyan@licp.cas.cn

[b] Key Laboratory for Electronic Materials of the State Ethnic Affairs Commission, College of Electric Engineering, Northwest University for Nationalities, Lanzhou, 730030, PR China

†Electronic supplementary information (ESI) available.

‡These authors contributed equally to this work.

This file includes:

- **Fig. S1** XRD patterns of the NbN-600, p-NbN and NbN-800.
- **Fig. S2** Cycling performance of the NbN-800 at 0.1 A g^{-1}.
- **Fig. S3** CV curves of as-prepared p-NbN electrode at different sweep rates (2-100 mV s^{-1}).
- **Fig. S4** Electrochemical properties of p-NbN electrode with a relatively high loading mass of 1 mg: (a) CV curves at different scan rates. (b) Capacitive and diffusion-controlled contributions to charge storage at a sweep rate of 0.5 mV s^{-1} (the capacitive contribution to the total current is shown by the shaded region).
- **Fig. S5** Representative reversible charging-discharge curves of p-NbN at different current rates of 0.1-2.0 A g^{-1} within the potential widow of 0.01-3 V (*vs.* Li/Li^+).
- **Fig. S6** (a) The 1^{st}, 2^{nd}, 3^{rd}, 10^{th} and 100^{th} charge-discharge curves of the raw Nb_2O_5 at 0.1 A g^{-1} within the potential widow of 1.1-3 V (*vs.* Li/Li^+). (b) Cycling performance of the Nb_2O_5 at 0.1 A g^{-1}.
- **Fig. S7** (a) The first discharge-charge profile of p-NbN electrode at 0.1 A g^{-1} within the potential widow of 0.01-3 V (*vs.* Li/Li^+). (b) Ex-situ XRD patterns obtained at various states of the discharge-charge process to understand the structural change upon battery operations.
- **Fig. S8** (a) CV curves of APDC within the potential region of 3-4.5 V (*vs.* Li/Li^+). (b) GCD curves of APDC at different current densities.
- **Fig. S9** (a) GCD curves of p-NbN//APDC LIHCs (p-NbN: APDC=1:1) within the potential regions of 0-4.5 V and 0-4.2 V at 0.1 A g^{-1}. (b) Cycling performance of p-NbN//APDC LIHC within the potential region of 0-4.2 V at a current rate of 1.0 A g^{-1}.
- **Fig. S10** GCD curves of p-NbN//APDC LIHCs based on p-NbN and APDC with different mass ratios (p-NbN: APDC=3:1~1:3).

- **Fig. S11** Ragone plots of p-NbN//APDC LIHCs based on p-NbN and APDC with different mass ratios (p-NbN: APDC=3:1~1:3).
- **Fig. S12** The IR drops identified in GCDs curves.
- **Fig. S13** (a) TEM image (insert: the selected area electron diffraction pattern) and (b) HR-TEM image of p-NbN in p-NbN//APDC LIHC after 15000 cycles at a current density of 1.0 A g^{-1}.
- **Fig. S14** The cross-section SEM images of the NbN electrode in p-NbN//APDC LIHC (a) before and (b) after 15000 cycles at a current density of 1.0 A g^{-1}.
- **Fig. S15** Nyquist plots of p-NbN//APDC LIHC before cycling, after 100 cycles and after 15000 cycles at the current density of 1.0 Ag^{-1}. Inset shows the data of high frequency range.
- **Fig. S16** A comparison of our p-NbN//APDC LIHC with other reported different types of supercapacitors: (1) Fe_2O_3@GNS//APDC in an ionic liquid electrolyte;[S5] (2) AC//MnO_2 in an ionic liquid electrolyte;[S6] (3) porous graphene//$Ni(OH)_2$@GNS in an aqueous KOH electrolyte;[S7] (4) APDC//APDC in a Li^+ organic electrolyte;[27] (5) Graphene/MnO_2//ACN in a Na_2SO_4 aqueous electrolyte;[S8] (6) V_2O_5//AC in a K_2SO_4 aqueous electrolyte;[S9] (7) CuO//AC in a KOH aqueous electrolyte;[S10] (8) AC//AC in a Na_2SO_4 aqueous electrolyte;[S11] (9) VN//VN in a KOH aqueous electrolyte.[43]
- Notes and references

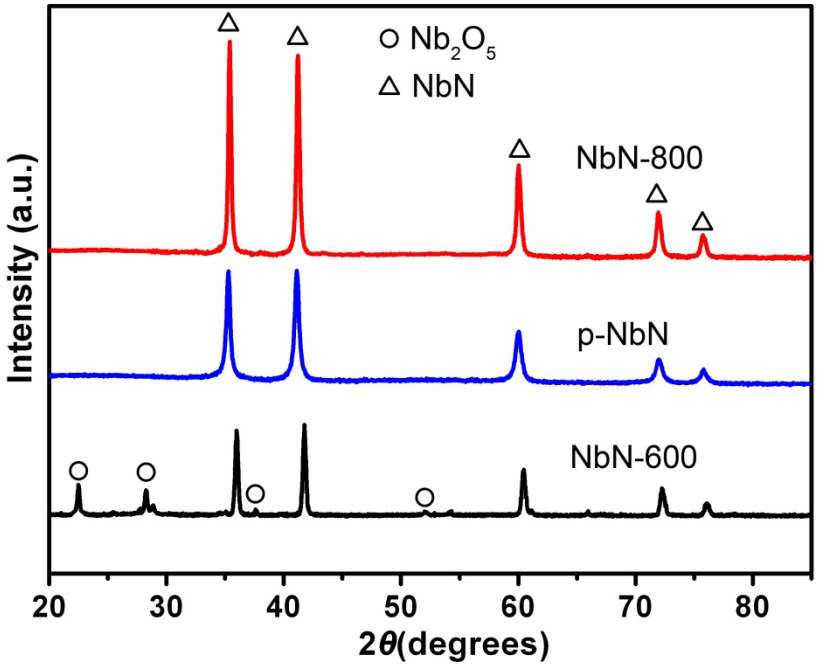

Fig. S1 XRD patterns of the NbN-600, p-NbN and NbN-800.

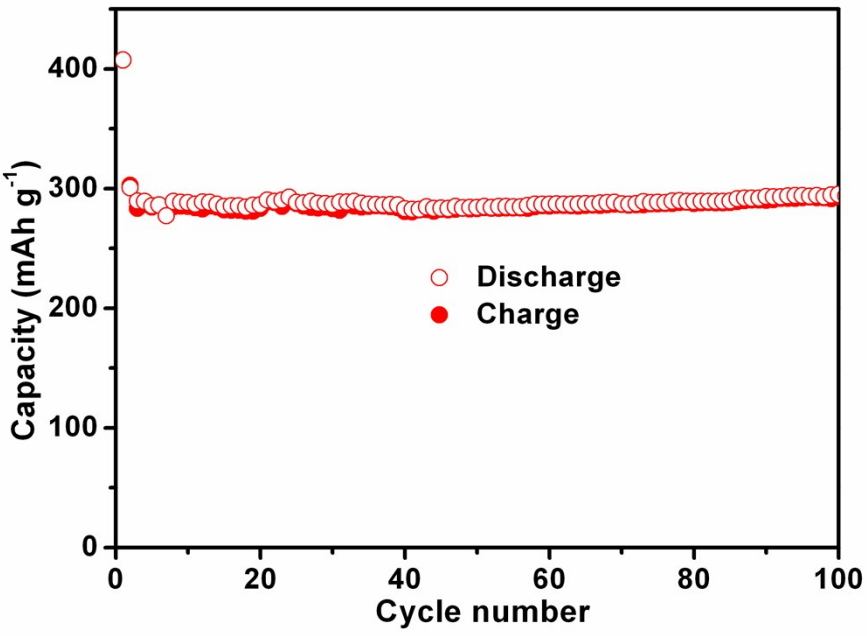

Fig. S2 Cycling performance of the NbN-800 at 0.1 A g^{-1}.

As seen from Fig. S1, NbN-600 contains composite structure of NbN and Nb_2O_5, indicating the incompletely conversion from Nb_2O_5 to NbN at 600 °C. NbN-800 shows a typical cubic NbN structure with larger grain size compared with that of p-

NbN prepared at 700 °C. Form Fig. S2 and Fig. 3f, it can be found that the reversible capacity of p-NbN is higher than that of NbN-800. According the reasons mentioned above, we chose 700 °C as the nitridation temperature.

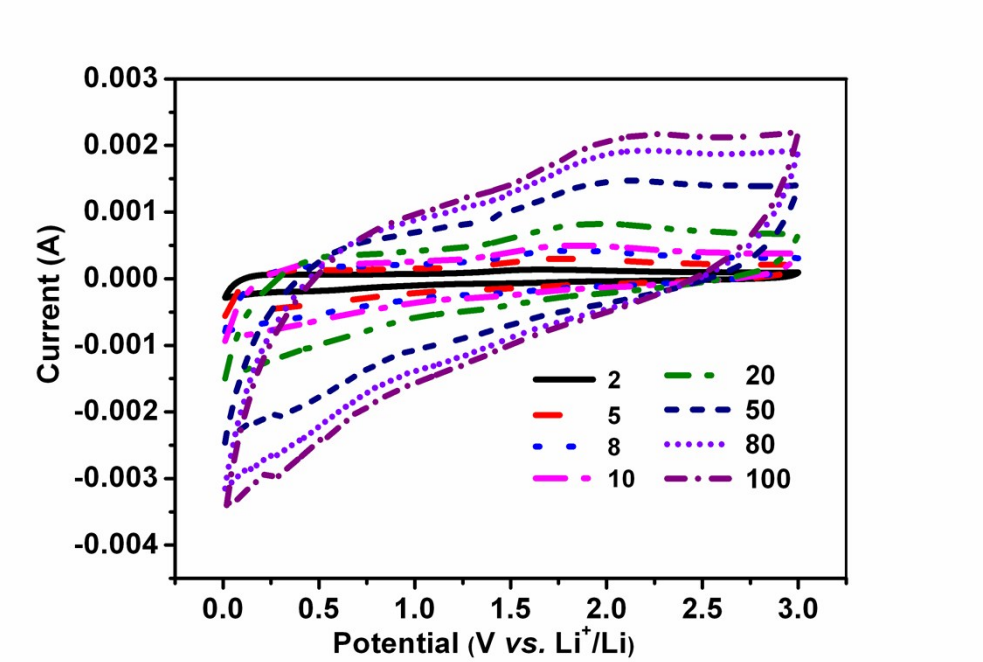

Fig. S3 CV curves of as-prepared p-NbN electrode at different sweep rates (2-100 mV s^{-1}).

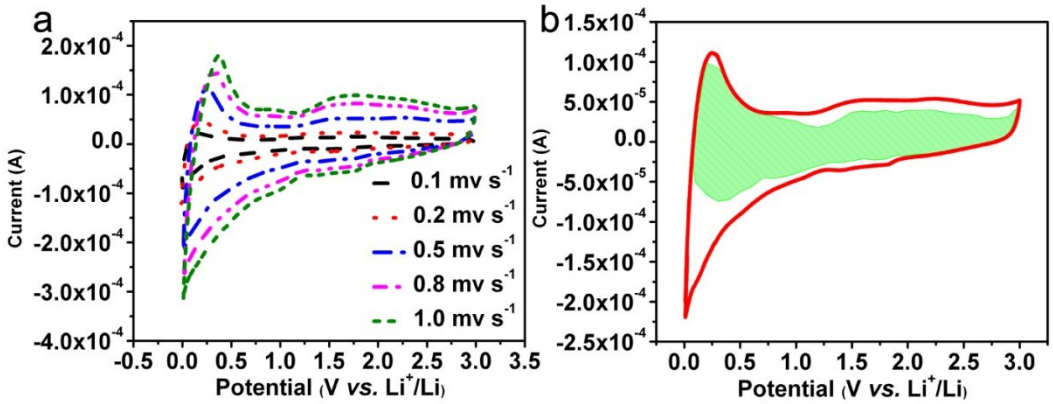

Fig. S4 Electrochemical properties of the great quality p-NbN electrode (1 mg per 1 cm^2): (a) CV curves at different scan rates. (b) Capacitive and diffusion-controlled contributions to charge storage at a sweep rate of 0.5 mV s^{-1} (the capacitive contribution to the total current is shown by the shaded region).

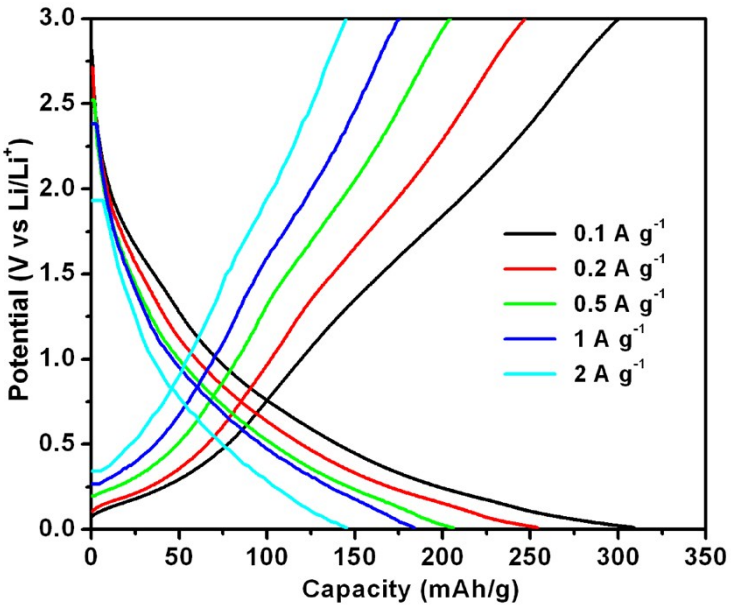

Fig. S5 Representative reversible charging-discharge curves of p-NbN at different current rates of 0.1-2.0 A g^{-1} within the potential widow of 0.01-3 V (*vs.* Li/Li^+).

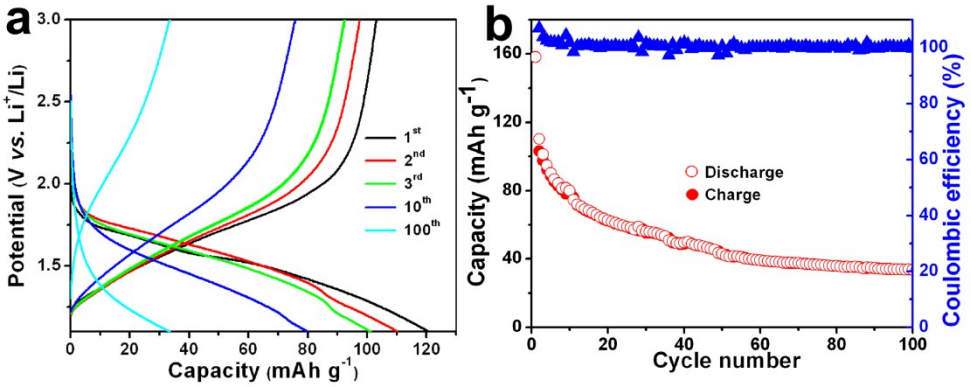

Fig. S6 (a) The 1st, 2nd, 3rd, 10th and 100th charge-discharge curves of the raw Nb_2O_5 at 0.1 A g^{-1} within the potential widow of 1.1-3 V (*vs.* Li/Li^+). (b) Cycling performance of the Nb_2O_5 at 0.1 A g^{-1}.

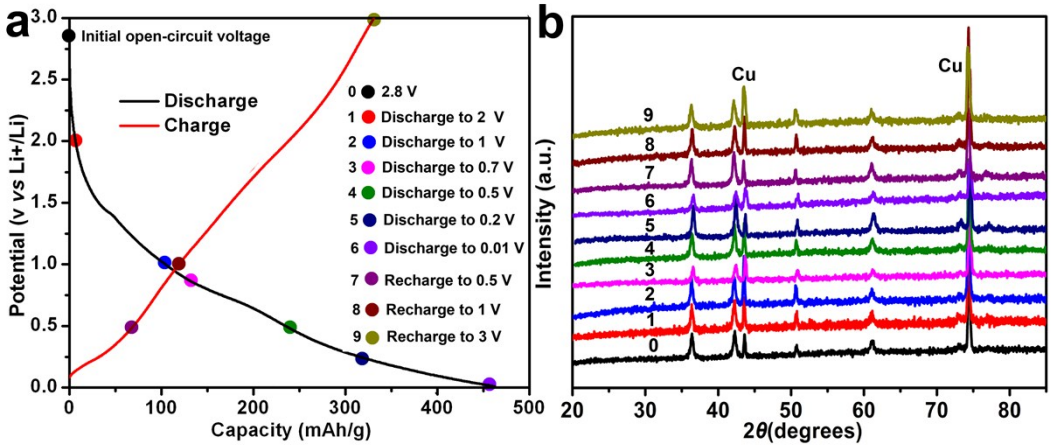

Fig. S7 (a) The first discharge-charge profile of p-NbN electrode at 0.1 A g^{-1} within the potential widow of 0.01-3 V (*vs.* Li/Li^+). (b) Ex-situ XRD patterns obtained at various states of the discharge-charge process to understand the structural change upon battery operations.

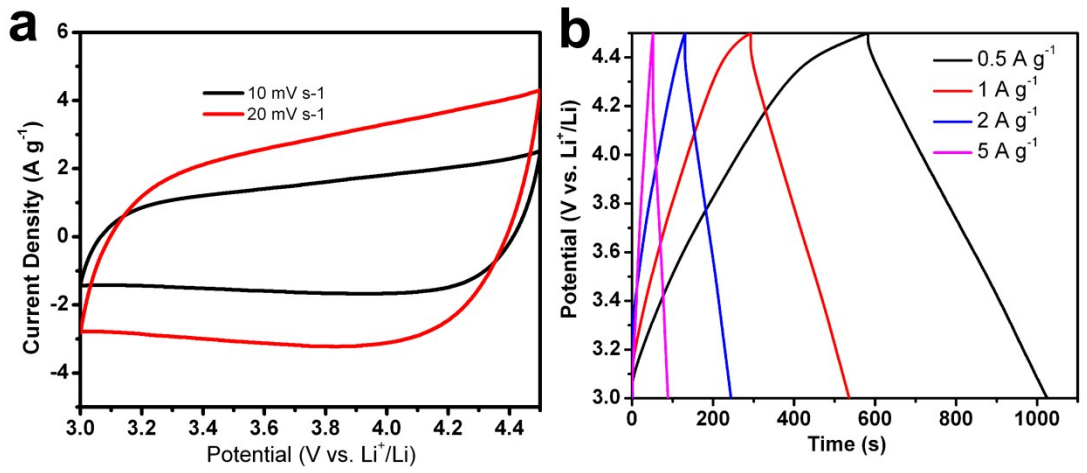

Fig. S8 (a) CV curves of APDC within the potential region of 3-4.5 V (*vs.* Li/Li$^+$). (b) GCD curves of APDC at different current densities.

Activated polyaniline derived carbon (APDC) was prepared by carbonization and followed by KOH action of the polyaniline nanorods.[S1-S4] As expected, APDC has an excellent electrochemical performance in organic electrolyte. Fig. S4a shows the CV curves of APDC electrode over 3.0-4.5 V (*vs.* Li/Li$^+$) in a Li half-cell system. The CV curves are relatively rectangular in shape and the charge-discharge curves are nearly straight lines (Fig. S4b), indicating a standard capacitive behavior of electrical double layer capacitance (EDLC). The APDC electrode displays a high capacity of ~148 F g^{-1} (~62 mAh g^{-1}) at 0.5 A g^{-1}.

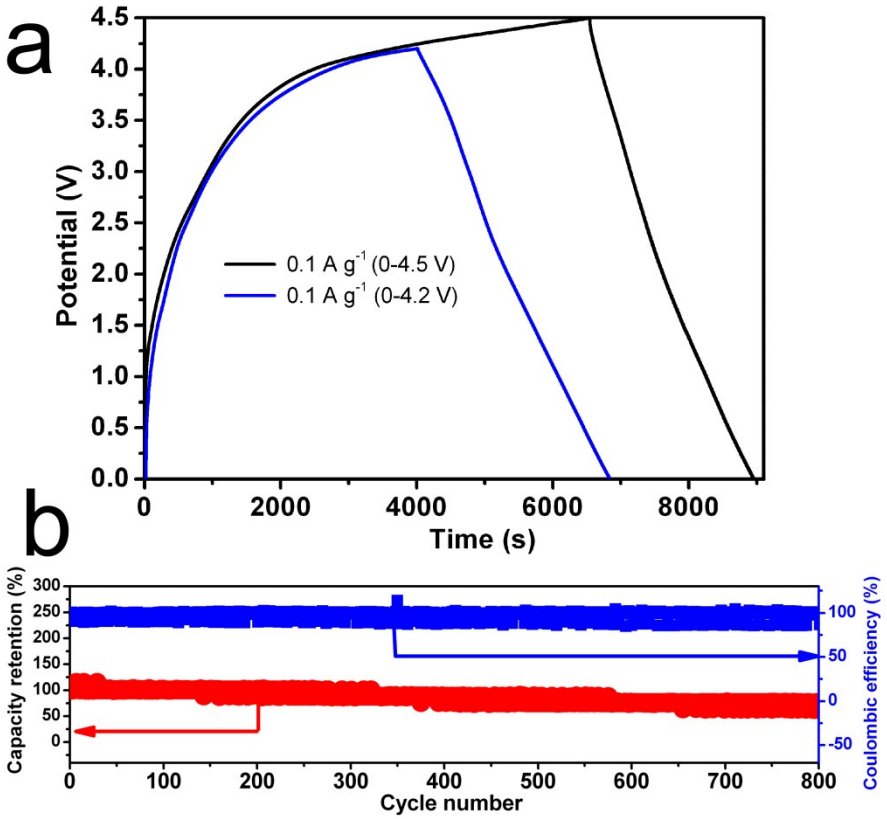

Fig. S9 (a) GCD curves of p-NbN//APDC LIHCs (p-NbN: APDC=1:1) within the potential regions of 0-4.5 V and 0-4.2 V at 0.1 A g^{-1}. (b) Cycling performance of p-NbN//APDC LIHC within the potential region of 0-4.2 V at a current rate of 1.0 A g^{-1}.

We also measured the GCD curves of p-NbN//APDC LIHCs (p-NbN: APDC=1:1) within the potential region of 0-4.5 V and 0-4.2 V, respectively. It can be found that the polarization phenomenon becomes obvious and the efficiency of charge-discharge is relatively low when the potential window increases to 0-4.5 V (Fig. S9a). In addition, we found that the potential window of the full cell could directly affect the cycle stability. The cycling performance is very poor when the potential window is 0-4.5 V (the date are not shown here). When the potential window is 0-4.2 V, the corresponding LIHC exhibits cycling a ~80% capacity retention after 800 cycles at 1.0 A g^{-1} (shown in Fig. S9b). In comparison, when the potential window is 0-4 V, the

corresponding LIHC exhibits superior long-term cycling stability with ~95% capacity retention after 15000 cycles at 1.0 A g^{-1} (shown in Fig. 4e). In view of the above reasons, we set 0-4 V as the potential window in the full cell.

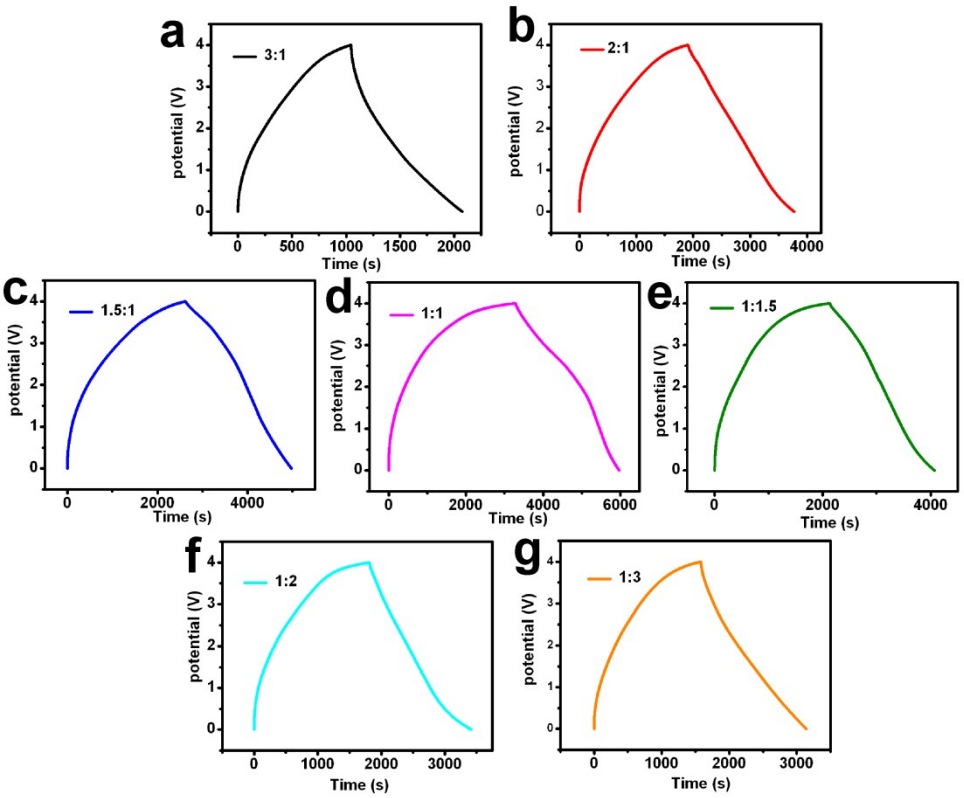

Fig. S10 GCD curves of p-NbN//APDC LIHCs based on p-NbN and APDC with different mass ratios (p-NbN: APDC=3:1~1:3).

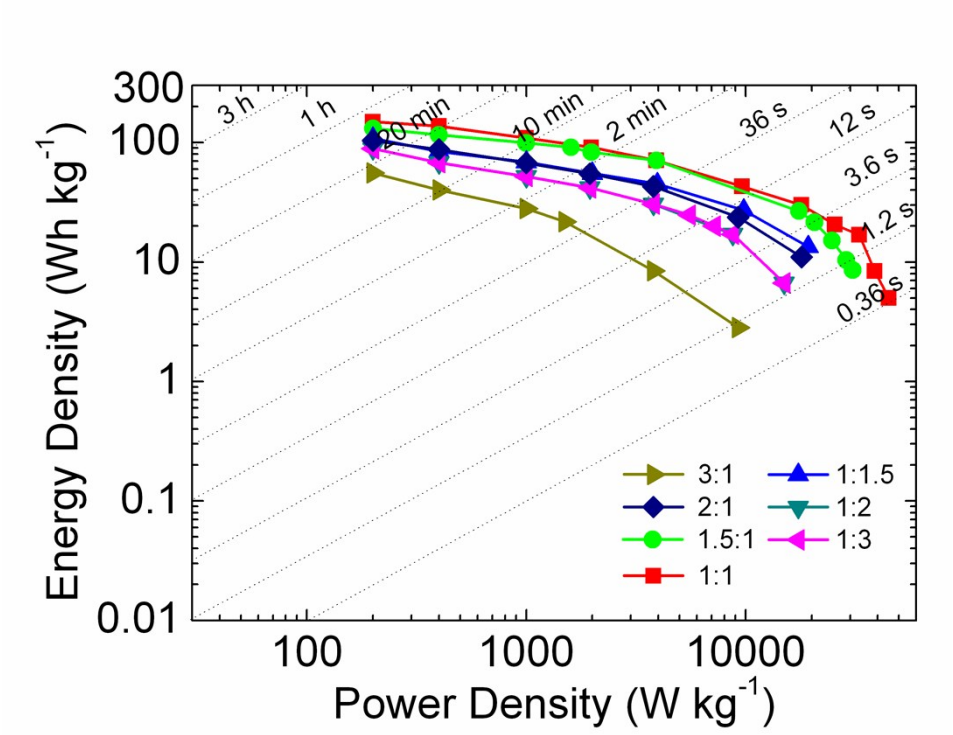

Fig. S11 Ragone plots of p-NbN//APDC LIHCs based on p-NbN and APDC with different mass ratios (p-NbN: APDC=3:1~1:3).

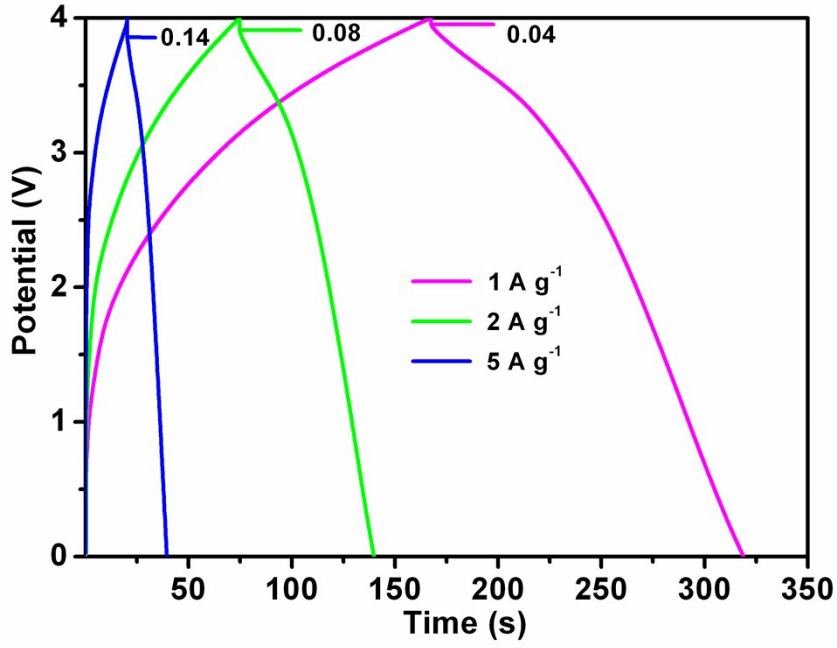

Fig. S12 The IR drops identified in GCDs curves.

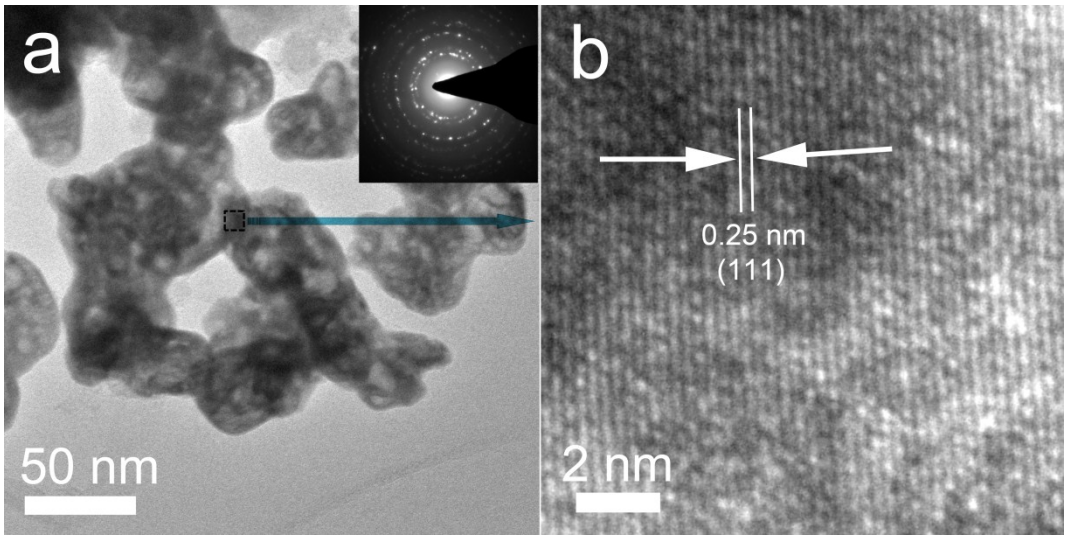

Fig. S13 (a) TEM image (insert: the selected area electron diffraction pattern) and (b) HR-TEM image of p-NbN in p-NbN//APDC LIHC after 15000 cycles at a current density of 1.0 A g^{-1}.

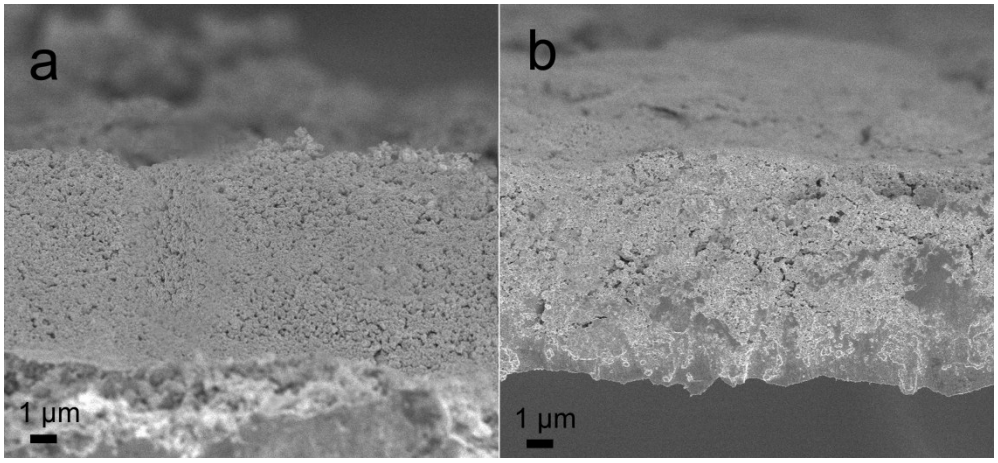

Fig. S14 The cross-section SEM images of the NbN electrode in p-NbN//APDC LIHC (a) before and (b) after 15000 cycles at a current density of 1.0 A g^{-1}.

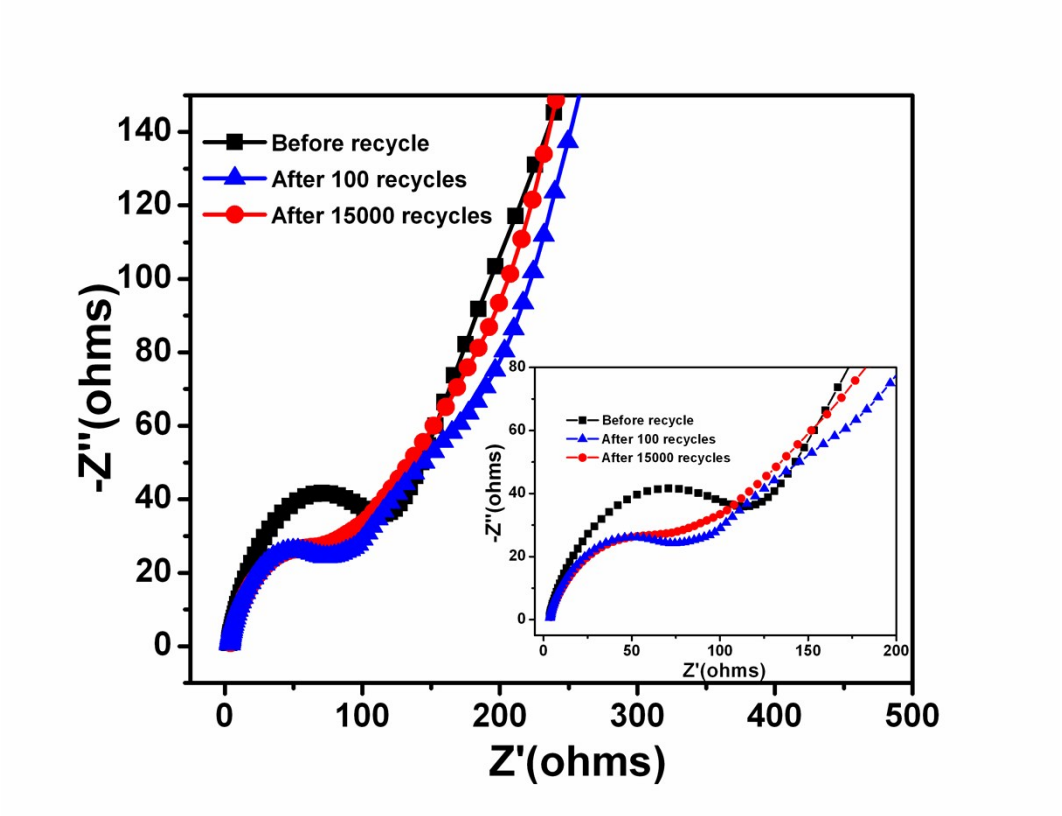

Fig. S15 Nyquist plots of p-NbN//APDC LIHC before cycling, after 100 cycles and after 15000 cycles at the current density of 1.0 Ag^{-1}. Inset shows the data of high frequency range.

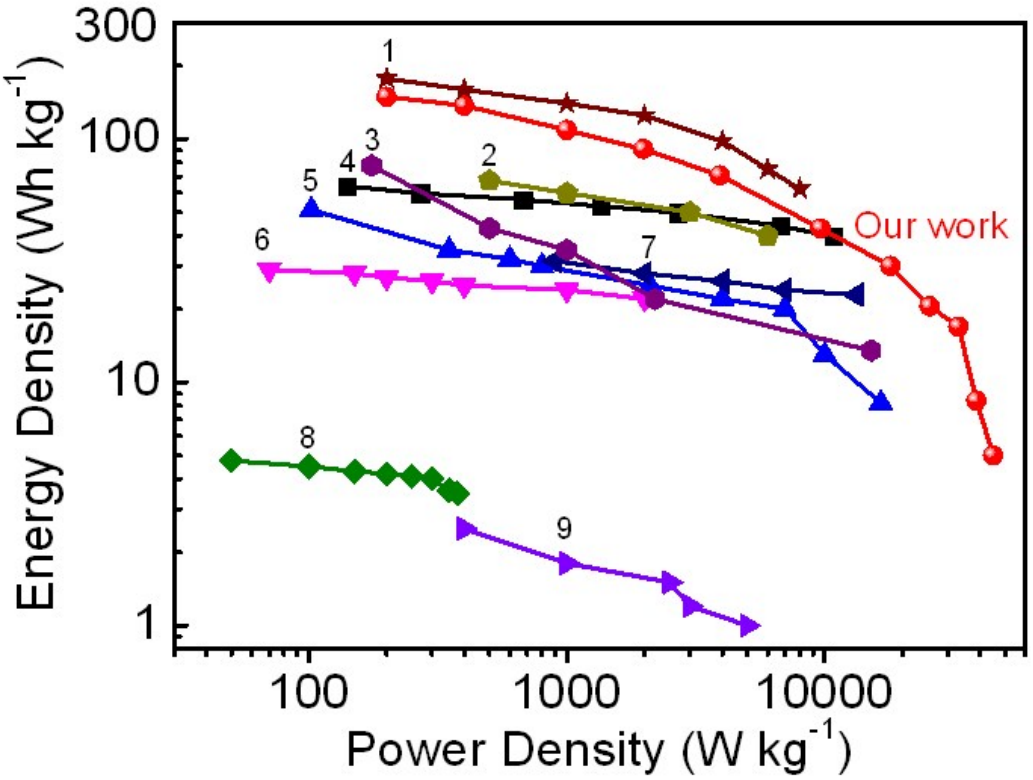

Fig. S16 A comparison of our p-NbN//APDC LIHC with other reported different types of supercapacitors: (1) Fe_2O_3@GNS//APDC in an ionic liquid electrolyte;[S5] (2) AC//MnO_2 in an ionic liquid electrolyte;[S6] (3) porous graphene//$Ni(OH)_2$@GNS in an aqueous KOH electrolyte;[S7] (4) APDC//APDC in a Li^+ organic electrolyte;[27] (5) Graphene/MnO_2//ACN in a Na_2SO_4 aqueous electrolyte;[S8] (6) V_2O_5//AC in a K_2SO_4 aqueous electrolyte;[S9] (7) CuO//AC in a KOH aqueous electrolyte;[S10] (8) AC//AC in a Na_2SO_4 aqueous electrolyte;[S11] (9) VN//VN in a KOH aqueous electrolyte.[43]

Furthermore, this integrated performance (energy density *vs.* power density) of our LIHC is higher than other reported different types of supercapacitors summarized in Fig. S16, including supercapacitors using an ionic liquid electrolytes such as Fe_2O_3@GNS//APDC and AC//MnO_2;[S5-S6] including Li^+ organic electrolyte symmetric supercapacitors such as APDC//APDC;[27] including aqueous supercapacitors such as porous graphene//$Ni(OH)_2$@GNS, Graphene/MnO_2//ACN, V_2O_5//AC, CuO//AC, AC//AC and VN//VN.[S7-S11,27,43]

Notes and references

S1 R. Wang, J. Lang, P. Zhang, Z. Lin and X. Yan, *Adv. Funct. Mater.*, 2015, **25**, 2270-2278.

S2 R. Wang, J. Lang and X. Yan, *Sci. China Chem.*, 2014, **57**, 1570-1578.

S3 R. T. Wang and X. B. Yan, *Sci. Rep*., 2014, **4**, 3712(1-9).

S4 Z. Chen, V. Augustyn, J. Wen, Y. Zhang, M. Shen, B. Dunn and Y. Lu, *Adv. Mater*., 2011, **23**, 791-795.

S5 S. Sun, J. Lang, R. Wang, L. Kong, X. Li and X. Yan, *J. Mater. Chem. A*, 2014, **2**, 14550-14556.

S6 X. Zhang, D. D. Zhao, Y. Q. Zhao, P. Y. Tang and Y. L. Shen, *J. Mater. Chem. A*, 2013, **1**, 3706-3712.

S7 J. Yan, Z. J. Fan, W. Sun and G. Q. Ning, *Adv. Funct. Mater.*, 2012, **22**, 2632-2641.

S8 Z. Fan , J. Yan , T. Wei , L. Zhi , G. Ning , T. Li and F. Wei, *Adv. Funct. Mater.*, 2011, **21**, 2366-2375.

S9 Q. T. Qu, Y. Shi, L. L. Li, W. L. Guo, Y. P. Wu, H. P. Zhang, S. Y. Guan, R. Holze, *Electrochem. Commun.*, 2009, **11**, 1325-1328.

S10 J. Zhang, H. Feng, Q. Qin, G. Zhang, Y. Cui, Z. Chai and W. Zheng, *J. Mater. Chem. A*, 2016, **4**, 6357-6367.

S11 C. Zheng, L. Qi, M. Yoshioc, H. Wang, *J. Power Sources*, 2010, **195**, 4406-4409.